Production cross section and decay study of ^{243}Es and ^{249}Md

R. Briselet,[1] Ch. Theisen,[1,*] M. Vandebrouck,[1] A. Marchix,[1] M. Airiau,[1] K. Auranen,[2,†] H. Badran,[2] D. Boilley,[3,4] T. Calverley,[2,5] D. Cox,[2,5,‡] F. Déchery,[1,6] F. Defranchi Bisso,[2] A. Drouart,[1] B. Gall,[6] T. Goigoux,[1] T. Grahn,[2] P. T. Greenlees,[2] K. Hauschild,[7] A. Herzan,[2,§] R. D. Herzberg,[5] U. Jakobsson,[2,‖] R. Julin,[2] S. Juutinen,[2] J. Konki,[2,¶] M. Leino,[2] A. Lightfoot,[2] A. Lopez-Martens,[7] A. Mistry,[5,#] P. Nieminen,[2,**] J. Pakarinen,[2] P. Papadakis,[2,5] J. Partanen,[2] P. Peura,[2] P. Rahkila,[2] J. Rubert,[6] P. Ruotsalainen,[2] M. Sandzelius,[2] J. Saren,[2] C. Scholey,[2] J. Sorri,[2,††] S. Stolze,[2,†] B. Sulignano,[1] J. Uusitalo,[2] A. Ward,[5] and M. Zielińska[1]

[1]*Irfu, CEA, Université Paris-Saclay, F-91191 Gif-sur-Yvette, France*

[2]*Department of Physics, University of Jyvaskyla, P.O. Box 35, FI-40014 Jyvaskyla, Finland*

[3]*Grand Accélérateur National d'Ions Lourds (GANIL), CEA/DSM - CNRS/IN2P3, Bd Henri Becquerel, BP 55027, F-14076 Caen Cedex 5, France*

[4]*Normandie Université, UNICAEN, Caen, France*

[5]*Department of Physics, University of Liverpool, Oliver Lodge Laboratory, Liverpool L69 7ZE, United Kingdom*

[6]*Institut Pluridisciplinaire Hubert Curien, F-67037 Strasbourg, France*

[7]*CSNSM, IN2P3-CNRS, F-91405 Orsay Campus, France*

(Received 28 September 2018; published 14 February 2019)

In the study of the odd-Z, even-N nuclei ^{243}Es and ^{249}Md, performed at the University of Jyväskylä, the fusion-evaporation reactions ^{197}Au(^{48}Ca, $2n$)^{243}Es and ^{203}Tl(^{48}Ca, $2n$)^{249}Md have been used for the first time. Fusion-evaporation residues were selected and detected using a gas-filled separator coupled with its focal-plane spectrometer. For ^{243}Es, the recoil decay correlation analysis yielded a half-life of 24 ± 3 s and a maximum production cross section of 37 ± 10 nb. In the same way, a half-life of 26 ± 1 s, an α-branching ratio of $75 \pm 5\%$, and a maximum production cross section of 300 ± 80 nb were determined for ^{249}Md. The decay properties of ^{245}Es, the daughter of ^{249}Md, were also measured: an α-branching ratio of $54 \pm 7\%$ and a half-life of 65 ± 6 s. Experimental cross sections were compared to the results of calculations performed using the KEWPIE2 statistical fusion-evaporation code.

DOI: 10.1103/PhysRevC.99.024614

I. INTRODUCTION

Determining the boundaries of the nuclear chart, particularly, in the region of superheavy nuclei (SHN), is one of the key questions driving fundamental nuclear physics. The SHN owe their existence to shell effects as without them the Coulomb repulsion would make the nuclei beyond $Z = 104$ unstable against fission [1]. In this context, detailed spectroscopy of very heavy nuclei (VHN) and SHN is of paramount importance to provide information on the nuclear landscape close to the high-A limit of the nuclear chart as well as on the nature of the predicted island of stability. The challenge of these experiments is related to low production cross sections and, in odd-mass nuclei, to the complexity of spectra where various collective and single-particle excitations may lie close in energy. On the other hand, the studies of odd-mass nuclei are rewarded by the wealth of information regarding single-particle states, exceeding what can be obtained for even-even nuclei [2].

Regarding the known excited states of single-particle or collective nature, little data is available for Es ($Z = 99$) and Md ($Z = 101$) isotopes [2,3]. Before in-beam spectroscopy of these odd-Z nuclei can be attempted, feasibility studies are a prerequisite, in particular, measurements of production cross sections. Such measurements also help to improve the description of the fusion-evaporation reaction mechanism, providing new constraints for the models.

In this paper, the production cross sections for ^{243}Es and ^{249}Md populated directly in the fusion-evaporation reactions

*christophe.theisen@cea.fr

†Present address: Physics Division, Argonne National Laboratory, 9700 South Cass Avenue, Lemont, Illinois 60439, USA.

‡Present address: University of Lund, Box 118, 221 00 Lund, Sweden.

§Present address: Institute of Physics, Slovak Academy of Sciences, SK-84511 Bratislava, Slovakia.

‖Present address: Department of Chemistry, Laboratory of Radiochemistry, University of Helsinki, P.O. Box 55, FI-00014 Finland.

¶Present address: CERN, CH-1211 Geneva 23, Switzerland.

#Present address: GSI Helmholtzzentrum für Schwerionenforschung GmbH, 64291 Darmstadt, Germany.

**Present address: Fortum Oyj, Power Division, P.O. Box 100, 00048 Fortum, Finland.

††Present address: Sodankylä Geophysical Observatory, University of Oulu, 90014 Oulu, Finland.

^{197}Au(^{48}Ca, $2n$)^{243}Es and ^{203}Tl(^{48}Ca, $2n$)^{249}Md are reported. The targets and projectiles were chosen as a compromise between the predicted production cross sections and the transmission in the separator. In particular, very asymmetric reactions using actinide targets were not considered as in such cases: (i) The large angular dispersion due to the low recoil velocity and neutron emission results in a poor transmission, (ii) the low recoil energy reduces the detection efficiency at the focal plane, both effects being not fully compensated by enhanced cross sections.

The present paper also allowed the half-lives and decay properties of these nuclei to be updated as well as those of ^{245}Es, populated by the α decay of ^{249}Md. It should be noted that α-decay branching ratios and, to a lesser extent, half-lives are needed to deduce production cross sections. Finally, the measured production cross sections for ^{243}Es and ^{249}Md are discussed in the context of the $Z \simeq 100$ region and compared to the predictions of the KEWPIE2 statistical fusion-evaporation code [4].

II. EXPERIMENTAL SETUP

The experiments were performed at the Accelerator Laboratory of the University of Jyväskylä (JYFL). The fusion-evaporation residues, including ^{243}Es and ^{249}Md, were separated from the fission fragments, the primary ^{48}Ca beam and the beam- and target-like reaction products using the recoil ion transport unit (RITU) gas-filled separator [5,6], which was operated at a He pressure of 0.4–0.6 mbars. The RITU transmission is estimated to be approximately 30% for the reactions considered here. The beam current was measured at regular intervals using a Faraday cup and monitored using the detectors counting rate, thus, allowing the beam dose to be deduced with an uncertainty of 20%.

At the focal plane of RITU, the separated fusion-evaporation residues were first detected in a position-sensitive multiwire proportional counter (MWPC) and then implanted in two adjacent double-sided silicon strip detectors (DSSDs), both detectors being part of the γ recoil electron α-tagging (GREAT) spectrometer [7]. The MWPC provided a time-of-flight (ToF) and energy loss (ΔE) measurement, allowing: (i) selection of the fusion-evaporation residues using a ToF-ΔE identification matrix and (ii) correlations with the DSSD, which enable the recoiling residues (coincidence) to be discriminated from the decay products (anticoincidence). Each DSSD is 300-μm thick and consists of 60×40 strips with a 1-mm strip pitch. The Y side of the DSSD was calibrated using an external mixed ^{239}Pu, ^{241}Am, and ^{244}Cm-α source. An energy offset is applied to account for the energy loss of the α particle in the detector entrance window (in the case of an external source) and for the daughter nucleus recoil (decay from the detector after implantation) so that the resulting energy corresponds to the literature value for the nuclei studied in the present paper. The X side was amplified with a higher gain to measure low-energy conversion electrons and calibrated using an external ^{133}Ba source. Signals from all detectors were processed by a triggerless acquisition system known as the total data readout [8]. The recoil decay correlation analysis was performed using the software package GRAIN [9]: After the first selection using the ToF-ΔE identification matrix, the fusion-evaporation residues (recoils) were identified using the energy of the α particles registered in the same pixel of the DSSD subsequent to the implantation of a recoil. The SAGE array [10] surrounded the target for the prompt γ and conversion-electron detection, however, data from this detector were not used in the present work.

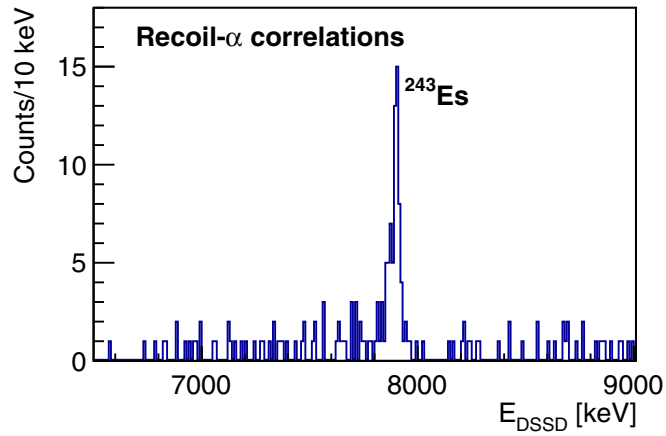

FIG. 1. α-particle energy spectrum of ^{243}Es measured in the DSSD resulting from recoil-α correlations using a maximum search time of 268 s.

III. ^{243}Es DECAY PROPERTIES AND PRODUCTION CROSS SECTION

A. Decay and half-life measurement

The ^{243}Es isotope was discovered in the 1970s by Eskola *et al.* using the ^{233}U(^{15}N, $5n$)^{243}Es reaction [11], and later revisited in the 1990 s by Hatsukawa *et al.* using the ^{233}U(^{14}N, $4n$)^{243}Es reaction [12]. A more recent study, performed with the SHIP separator at GSI by Antalic *et al.* [13], has shown that ^{243}Es decays to its daughter via an α particle with an energy of 7893 ± 10 keV with a half-life of $T_{1/2} = 23 \pm 3$ s and an α-decay branching ratio of $61 \pm 6\%$. An α-particle fine-structure was tentatively observed with peaks at 7745 ± 20 and 7850 ± 20 keV. In the work of Antalic *et al.* [13], ^{243}Es was populated in the decay of the mother nucleus ^{247}Md, whereas in the present paper, it was directly produced in the ^{197}Au(^{48}Ca, $2n$)^{243}Es reaction, with a 21-pnA ^{48}Ca beam at $\sim$210-MeV energy impinging on a ^{197}Au target. The ^{48}Ca + ^{197}Au reaction has already been studied in the 1990s by Gäggeler *et al.* [14], however, few spectroscopic data were available at that time, preventing the discrimination of fusion-evaporation residues from $2n$ and $3n$ channels.

Figure 1 presents the α-particle energy spectrum measured in the DSSD resulting from recoil-α correlations with the decay of ^{243}Es clearly visible.

The time distribution (ΔT) of the α decay with respect to the implantation, selecting the ^{243}Es α-decay energy, is presented in Fig. 2. In the inset, the time distribution is drawn as a function of $\ln(\Delta T)$ using a maximum search time of 10 h. The peak at $\ln(\Delta T) = 10.5$ corresponds to the ^{243}Es decay, whereas that around $\ln(\Delta T) = 16$ is related to random

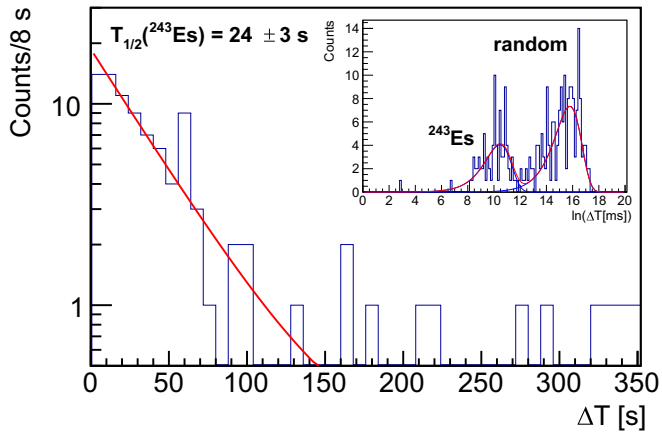

FIG. 2. Time distribution of α decays with respect to the ^{243}Es fusion-evaporation residue implantation. The inset shows the same data as a function of $\ln(\Delta T)$ with ΔT expressed in milliseconds. It should be noted that the range is different for the two spectra: 350 s for the main panel and 135 h for the inset. The fit using a two-component decay curve (real and random) is shown with a solid line.

correlations occurring at an average time interval of ≈5000 s. The spectrum in the main panel can be fitted using the function [15],

$$f(T) = Ae^{-(\lambda+r)\Delta T} + Be^{-r\,\Delta T}, \quad (1)$$

where λ is the decay constant of the nucleus of interest and r is the random correlation rate. Similarly, the spectrum in the inset can be fitted following the method described in Ref. [16]. As expected, both procedures give the same result, yielding the half-life of $T_{1/2} = 24 \pm 3$ s, in agreement with the results of the experiment performed at SHIP [13].

The inset of Fig. 2 demonstrates that the ^{243}Es decay events can be well separated from the background in the defined range of $\ln(\Delta T) < 12.5$, which corresponds to a time window of 268 s after the recoil implantation. This search time is used in the next section in order to determine the number of events corresponding to the α decay of ^{243}Es.

The recoil-α-α correlations were used to search for the decay of ^{239}Bk following the ^{243}Es decay. The negative outcome of this search is again consistent with the results of the measurement at SHIP [13]. The decay properties of nuclei studied in the present paper are summarized in Table I.

B. Production cross section

In order to study the production cross section for ^{243}Es using the fusion-evaporation reaction ^{197}Au(^{48}Ca, $2n$)^{243}Es, two different beam energies were used. The target used for this measurement was a 270 ± 13-μg cm^{-2}-thick ^{197}Au self-supporting foil. The cyclotron delivered a 213.0 ± 1.0-MeV beam first passing through the 100-μg cm^{-2} carbon window of the SAGE electron spectrometer. The first part of the study was performed with a beam energy in the middle of the target (MoT) estimated to be 210.0 ± 1.0 MeV. Then, a carbon degrader foil of 100 μg cm^{-2} was placed upstream to reduce the incident energy (MoT) to 208.0 ± 1.0 MeV. The spectrum presented in Fig. 1 corresponds to the total statistics, namely, with and without the degrader.

TABLE I. Summary of decay properties obtained in the present paper compared to the literature values.

Nucleus	Half-life (s)	α-decay branching ratio (%)	Reference
^{243}Es	24 ± 3	^{239}Bk not observed	This paper
	23 ± 3	61 ± 6	[13]
^{245}Es	65 ± 6	54 ± 7	This paper
		40 ± 10	[17]
	80^{+96}_{-28}	80^{+20}_{-50}	[18]
	66 ± 6		[12]
	$55^{+12}_{-8.4}$		[19]
^{249}Md	26 ± 1	75 ± 5	This paper
	25^{+14}_{-7}	>60	[18]
	19^{+3}_{-2}		[20]
	$23.8^{+3.8}_{-2.9}$		[19]
	23 ± 3		[21]
		75	[22]

The number of counts attributed to the ^{243}Es α decay was obtained using a maximum search time of 268 s. The contribution from random correlations was estimated by integrating the random correlations component [second term in Eq. (1) in the case $\lambda \gg r$] using this time window. After subtracting this background, the number of α particles stemming from ^{243}Es was determined to be 50 ± 7 (32 ± 6) without (with) the carbon degrader foil. The uncertainties were evaluated following the method described in Ref. [23]. In the present work, the statistics is large enough to consider standard normal distributions, therefore, symmetric uncertainties are adopted.

During the acquisition time without and with the degrader, the number of ^{48}Ca nuclei that impinged on the ^{197}Au target was equal to $(1.6 \pm 0.3) \times 10^{16}$ and $(1.2 \pm 0.2) \times 10^{16}$, respectively. Taking into account the ^{197}Au target thickness, the α-decay branching ratio of $61 \pm 6\%$ [13], the α-detection efficiency of 55%, and assuming a RITU transmission of 30%, a production cross section $\sigma(^{243}\text{Es}) = 37 \pm 10$ nb was deduced for a beam energy of 210.0 ± 1.0 MeV (without the degrader), and $\sigma(^{243}\text{Es}) = 32 \pm 9$ nb for a beam energy of 208.0 ± 1.0 MeV (with the degrader). Only statistical uncertainties corresponding to the beam dose, number of α particles, and α-decay branching ratio are given. The RITU transmission of 30% is actually a transmission × detection efficiency including the transmission through the separator, the time-of-flight, and the DSSD detection efficiencies. The results are presented in Table II.

TABLE II. Production cross sections for ^{243}Es using the fusion-evaporation reaction ^{197}Au(^{48}Ca, $2n$)^{243}Es measured for two different ^{48}Ca beam energies (E_{beam} corresponds to the middle of target). N_α is the number of observed α decays after background subtraction.

E_{beam} (MeV)	^{48}Ca dose	N_α	σ (nb)
210.0 ± 1.0	$(1.6 \pm 0.3) \times 10^{16}$	50 ± 7	37 ± 10
208.0 ± 1.0	$(1.2 \pm 0.2) \times 10^{16}$	32 ± 6	32 ± 9

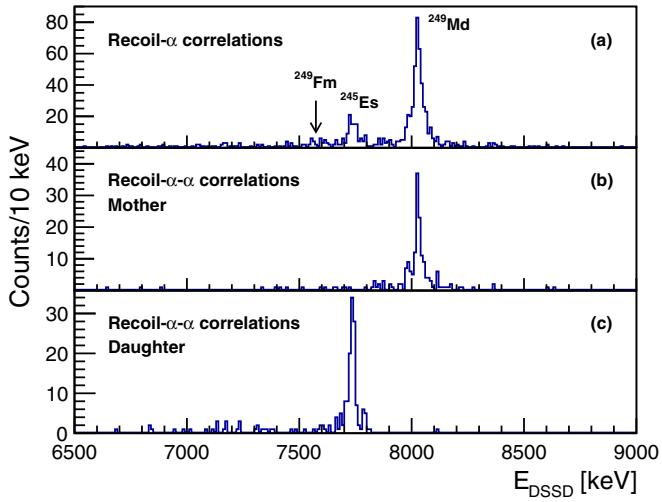

FIG. 3. α-particle energy spectra of ^{249}Md, ^{249}Fm and ^{245}Es resulting from (a) recoil-α and (b), (c) recoil-α-α correlations using a maximum search time of 10 min.

IV. ^{249}Md DECAY PROPERTIES AND PRODUCTION CROSS SECTION

The odd-Z nucleus ^{249}Md was populated using the fusion-evaporation reaction ^{203}Tl(^{48}Ca, $2n$)^{249}Md in three different irradiation campaigns. The first campaign was focused on cross-section measurements at two different bombarding energies of 214.3 ± 1.1 and 212.7 ± 1.1 MeV. The results are reported in Sec. IV B. The two subsequent campaigns aimed principally at the in-beam and decay spectroscopy of ^{249}Md, results of which will be reported in a forthcoming paper. The data collected in the three campaigns were used to derive the ^{245}Es and ^{249}Md half-lives and α-decay-branching ratios as presented in the following section.

A. ^{249}Md and ^{245}Es decay and half-life measurement

The α-particle energy spectra obtained using recoil-α and recoil-α-α correlations with the statistics of the three campaigns summed together are presented in Fig. 3. A maximum search time of 10 min after the identification of an implanted recoiling nucleus was used. ^{249}Md features an electron capture (EC)/β^+-decay branch feeding ^{249}Fm. The α decay of the latter is observed using recoil-α correlations since the detection system is insensitive to the β^+ particle [see panel (a) of Fig. 3]. The ^{245}Es α decay observed using recoil-α correlations corresponds to the events when the α particle emitted from ^{249}Md escapes from the DSSD without being detected. The α decay of ^{249}Fm is more clearly visible in Fig. 4, which represents the α-decay time on a logarithmic scale as a function of the α-particle energy. Using recoil-α-α correlations allows the mother ^{249}Md and daughter ^{245}Es α decays to be isolated as shown in the (b) and (c) panels of Fig. 3. From the literature, the α-particle energies are as follows: $E_\alpha(^{249}\text{Md}) = 8026 \pm 10$ keV [21], and $E_\alpha(^{245}\text{Es}) = 7730 \pm 1$ keV [12]. The satellite peaks in the α decay of ^{249}Md at 7956 and 8087 keV, suggested in Ref. [21], are also tentatively observed in the present paper.

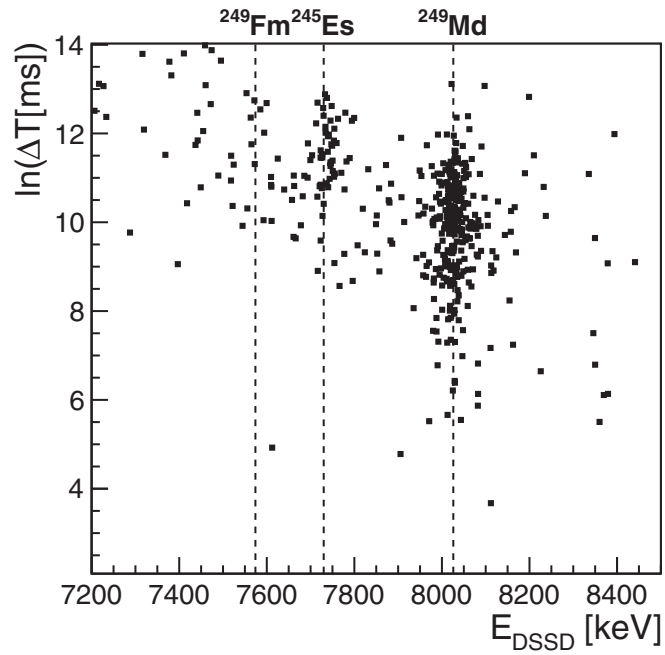

FIG. 4. α-decay time distribution on a logarithmic scale (from ~7 ms to ~20 min) as a function of the decay energy.

Figure 5 shows the time distribution of the ^{249}Md α decay with respect to the implantation time. The distribution plotted as a function of $\ln(\Delta T)$ for a maximum search time of 24 h is shown in the inset. As shown in this plot, the random correlations are negligible, therefore, the time distribution displayed in the main panel can be fitted with a single exponential function. A half-life of $T_{1/2} = 26 \pm 1$ s is obtained using a maximum search time of 300 s. This value can be compared with previously measured half-lives. The ^{249}Md decay has been studied at SHIP by Heßberger and co-workers following the α decay of ^{257}Db($\rightarrow$ ^{253}Lr $\rightarrow$ ^{249}Md) [18,20]

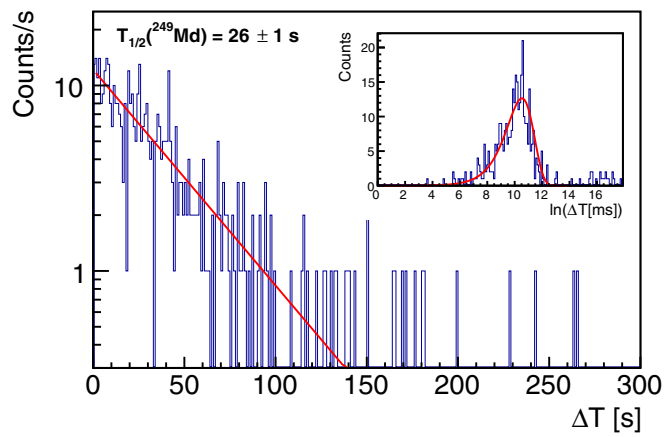

FIG. 5. Time distribution of α decays with respect to the ^{249}Md fusion-evaporation residue implantation. The inset shows the same data as a function of $\ln(\Delta T)$ with ΔT expressed in milliseconds. It should be noted that the range is different for the two spectra: 300 s for the main panel and 18.2 h for the inset. The fit using a one-component decay curve is shown with a solid line.

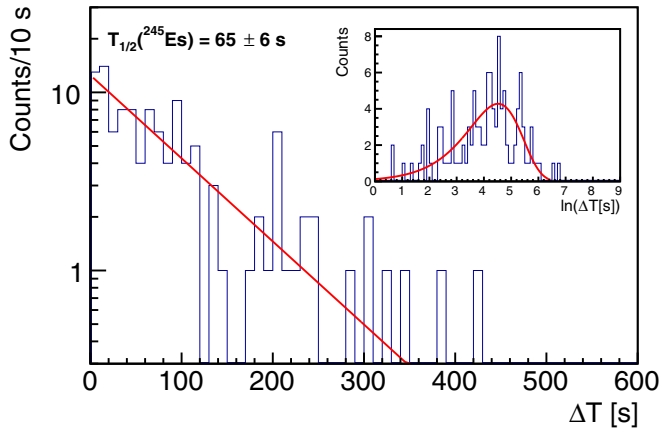

FIG. 6. Time distribution of the α decay of ^{245}Es with respect to the ^{249}Md α decay. The inset shows the same data as a function of $\ln(\Delta T)$ with ΔT expressed in seconds. It should be noted that the range is different for the two spectra: 600 s for the main panel and 2.25 h for the inset. The fit using a one-component decay curve is shown with a solid line.

and the α decay of ^{253}Lr [21] and by Gates *et al.* using the Berkeley gas-filled separator following the α decay of ^{257}Db [19]. Our revised half-life of ^{249}Md obtained via direct production and with higher statistics is compatible with the values obtained in these works: 25^{+14}_{-7} s [18], 19^{+3}_{-2} s [20], 23 ± 3 s [21], $23.8^{+3.8}_{-2.9}$ s [19]; see also Table I.

Similarly, Fig. 6 presents the time distribution of the ^{245}Es α decay with respect to that of ^{249}Md, the time represented in linear and as a function of $\ln(\Delta T)$ scales. Again, the background is found to be negligible. The distribution was then fitted with a single component. The half-life $T_{1/2}(^{243}\text{Es}) = 65 \pm 6$ s was extracted, a value compatible with those obtained by Heßberger *et al.* following the α decay of ^{257}Db($\rightarrow$ ^{253}Lr $\rightarrow$ ^{249}Md $\rightarrow$ ^{245}Es): 80^{+96}_{-28} s [18], by Hatsukawa *et al.* after direct synthesis using the fusion-evaporation reactions ^{238}U(^{14}N, $7n$)^{245}Es and ^{237}Np(^{12}C, $4n$)^{245}Es: 66 ± 6 s [12], and by Gates *et al.* following the α decay of ^{257}Db: $55^{+12}_{-8.4}$ s [19]; see also Table I.

The α-decay-branching ratio of ^{249}Md is defined as the ratio of the α-decay branch to ^{245}Es, to the total decay strength, including the EC/β^+ branch to ^{249}Fm. The latter is evaluated using the number of events attributed to the ^{249}Fm α decay from Figs. 3 and 4, corrected for the ^{249}Fm α-decay-branching ratio. A correction is also applied to take into account the fraction of ^{249}Fm nuclei that decay during the search time of 600 s. The ^{249}Fm half-life of 2.6 ± 0.7 min is taken from the evaluated data [24]. The ^{249}Fm α-decay branching ratio of $15.6 \pm 1.0\%$ is taken from Heßberger *et al.* [25], which is more recent than the evaluation of Ref. [24].[1] The resulting α-decay-branching ratio deduced in the present work is $b_\alpha(^{249}\text{Md}) = 75 \pm 5\%$. The evaluated value of $b_\alpha(^{249}\text{Md}) > 60\%$ [24] corresponds to the measurement of Heßberger *et al.*, which has been obtained in the study of the ^{257}Db decay chain [18]. A more recent value of $b_\alpha(^{249}\text{Md}) = 75\%$, quoted without uncertainty in the Ph.D. thesis of Streicher [22], is in perfect agreement with our measurement; see also Table I.

The α-decay-branching ratio of ^{245}Es can be extracted in two distinct ways. The first possibility is to derive it as the ratio of the number of events corresponding to ^{249}Md obtained using recoil-α-α and recoil-α correlations, corrected for the DSSD efficiency for a full-energy measurement $\epsilon_\alpha = 55\%$ under the condition that the recoil-α-α correlations are obtained by gating on the full-energy peaks only,

$$b_\alpha(^{245}\text{Es}) = \frac{N_{\text{recoil-}\alpha\text{-}\alpha}(^{249}\text{Md})}{N_{\text{recoil-}\alpha}(^{249}\text{Md})} \frac{1}{\epsilon_\alpha}. \quad (2)$$

The second option is to obtain it as the ratio of counts corresponding to ^{245}Es and ^{249}Md in the total α-particle spectrum. Both methods lead to the same value of $b_\alpha(^{245}\text{Es}) = 54 \pm 7\%$. For comparison, the previously reported values were $b_\alpha(^{245}\text{Es}) = 40 \pm 10\%$ (Eskola [17]), $b_\alpha(^{245}\text{Es}) = 80^{+20}_{-50}\%$ (Heßberger *et al.* [18]). The decay properties of ^{249}Md and ^{245}Es are summarized in Table I.

B. Production cross section

The fusion-evaporation reaction ^{203}Tl(^{48}Ca, $2n$)^{249}Md was studied at two different bombarding energies. The cyclotron delivered a 218-MeV beam first passing through the 100-μg cm^{-2} carbon window of the SAGE electron spectrometer. The ^{203}Tl target having a thickness of 318 ± 16 μg cm^{-2} was evaporated on a carbon foil of 20 μg cm^{-2} and covered by a 10-μg cm^{-2} carbon protection layer. The resulting energy in the middle of the ^{203}Tl target was estimated to be 214.3 ± 1.1 MeV. Using in addition an 80-μg cm^{-2} carbon degrader foil resulted in an energy of 212.7 ± 1.1 MeV MoT.

The spectra were obtained using a search time of 207 s, i.e., eight ^{249}Md half-lives. Contrary to the ^{243}Es case, the background was found to be negligible.

The total number of ^{48}Ca particles that impinged on the target was $(1.8 \pm 0.4) \times 10^{15}$ [$(1.5 \pm 0.3) \times 10^{15}$] for the measurement without (with) the carbon degrader foil. Using a ^{203}Tl target thickness of 318 ± 16 μg cm^{-2}, an α-branching ratio of $75 \pm 5\%$, a RITU transmission $\times$ detection efficiency of 30% and a full-energy α-detection efficiency of 55%, cross sections $\sigma(^{249}\text{Md})$ of 300 ± 80 and 70 ± 40 nb are deduced for the incident energies of 214.3 and 212.7 MeV, respectively. Again, only statistical uncertainties are given. The results are summarized in Table III.

V. DISCUSSION

In this section, we discuss the new cross-section measurements for ^{243}Es and ^{249}Md. These results are placed in the

[1] It should be noted that, in Ref. [25], the half-life of ^{249}Fm has not been remeasured. The value adopted in this reference is actually that of the evaluation of Ref. [24], i.e., 2.6 ± 0.7 min. In the most recent NUBASE2016 evaluation [26], the α-decay-branching ratio of ^{249}Fm is taken from Ref. [24] ($33 \pm 9\%$), whereas for the half-life only the value from Ref. [27] (96 ± 6 s) is selected.

TABLE III. Production cross sections for ^{249}Md using the fusion-evaporation reaction ^{203}Tl(^{48}Ca, $2n$)^{249}Md measured for two different ^{48}Ca beam energies (E_{beam} corresponds to the middle of the target).

E_{beam} (MeV)	^{48}Ca dose	N_α	σ (nb)
214.3 ± 1.1	$(1.8 \pm 0.4) \times 10^{15}$	68 ± 8	300 ± 80
212.7 ± 1.1	$(1.5 \pm 0.3) \times 10^{15}$	12 ± 4	70 ± 40

context of experimental cross sections for cold fusion-evaporation reactions and the $2n$ channel for $Z \approx 100$, presented in Fig. 7 and compared to new reactions dynamics calculations using the statistical fusion-evaporation code KEWPIE2 [4].

A. $2n$ channel fusion-evaporation systematics

It is generally acknowledged that the fusion-evaporation reactions can be described as three subsequent independent processes: capture, compound-nucleus formation, and survival of the residual nucleus. The description of the capture step is rather well controlled in terms of barrier penetration with no rapid evolution as a function of mass and charge when using similar projectiles and targets. The formation step results in a sharp decrease in the cross section for projectile-target combinations with $Z_p Z_t \gtrsim 1600$–1800, known as the fusion hindrance, which prevents the formation of a compound nucleus by leading the dinuclear composite towards the quasifission route. This effect starts to act in the region considered here, and it can account for the exponential decrease in the cross sections observed for larger Z values in Fig. 7. Consequently, only the survival step can account for the decrease in cross sections below $Z \approx 102$. The global trend displayed by the cross sections presented in Fig. 7 may be explained by a combination of two effects. First, the fourfold magic character of the $^{48}\text{Ca} + {}^{208}\text{Pb} \rightarrow {}^{256}\text{No}^*$ reaction leads to a low-Q value and, therefore, a higher survival probability in the evaporation and de-excitation processes. This enhancement is observed for ^{254}No and neighboring residual nuclei. Second, the semimagicity at $Z = 100$, $N = 152$ leads to higher shell corrections (higher fission barrier) and, therefore, a higher survival probability around ^{252}Fm. Note that, if the cross sections are plotted as a function of the mass or neutron number, they also display a bell-shaped behavior.

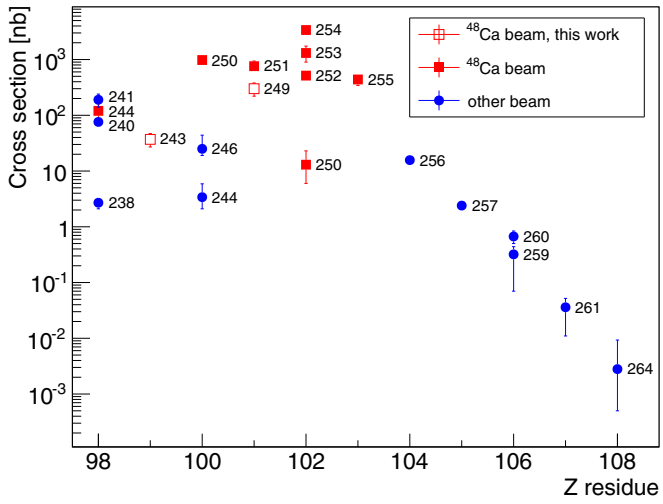

FIG. 7. Systematics of the fusion-evaporation cross sections in the $2n$ channel as a function of Z of the residual nucleus. The filled red squares correspond to reactions induced by a ^{48}Ca beam, whereas the blue circles correspond to those using other beams. The new ^{243}Es and ^{249}Md measurements are denoted by empty square symbols. The mass number A of the residual nucleus is given to the right of each symbol. Data are taken from Refs. [28] (^{238,240,241}Cf), [29] (^{244}Cf), this paper (^{243}Es, ^{249}Md), [30] (^{244,246}Fm), [31] (^{250}Fm), [32] (^{251}Md), [33] (^{250}No), [34] (^{252,253}No), [14] (^{254}No, ^{255}Lr), [35] (^{256}Rf), [20] (^{257}Db), [36] (^{259}Sg), [21] (^{260}Sg), [37] (^{261}Bh), [38] (^{264}Hs).

B. Cross-section calculations

In the following, the fusion-evaporation cross sections illustrated with the new experimental results for ^{243}Es and ^{249}Md are discussed in terms of survival from the compound to the residual nucleus with an emphasis on the effect of the fission barrier. The present measurements are performed in a mass region where the fusion hindrance is not yet significant. Consequently, the fusion process is modelled in the KEWPIE2 code by considering only the capture phase, which is computed using a proximity potential and the Wentzel-Kramers-Brillouin (WKB) approximation, see Ref. [4] for details.

The KEWPIE2 code [4] treats the competition between light-particle evaporation and fission, which occurs within an excited compound nucleus using the statistical formalisms of Weisskopf [41] and Bohr-Wheeler [42], respectively. The entire set of default parameters used in the KEWPIE2 code is presented in Ref. [4]. In the following, we will only focus on a few parameters, which are not well defined either theoretically or experimentally in this mass region [43]. These parameters are the reduced friction parameter β, the shell-damping energy E_d, and the shell corrections ΔE_{sh}. These parameters are related to the viscosity of nuclear matter, the stability of shell corrections with temperature, and the fission-barrier height, respectively, following Eq. (3) for the latter:

$$B_f = B_{\text{LDM}} - \Delta E_{\text{sh}}, \tag{3}$$

where B_f is the fission-barrier height and B_{LDM} is the liquid-drop fission barrier. The default values used in the KEWPIE2 code are $\beta = 2 \times 10^{21}$ s^{-1}, $E_d = 19$ MeV, whereas the finite-range droplet model (FRDM) ΔE_{sh} shell corrections are taken from Ref. [40]. It should be stressed that those parameters mainly affect the fission process that is known to be dominant for heavy and superheavy nuclei. Indeed, a small variation of the fission parameters, such as the strength of the dissipation or the fission-barrier heights, leads to a significant modification of the survival probability and, consequently, the related observables, in particular, the production cross sections.

Figure 8 presents the experimental results for the production cross sections for ^{243}Es and ^{249}Md (Tables II and III) compared to the calculations performed with the KEWPIE2 code using the default parameters. For ^{249}Md, the

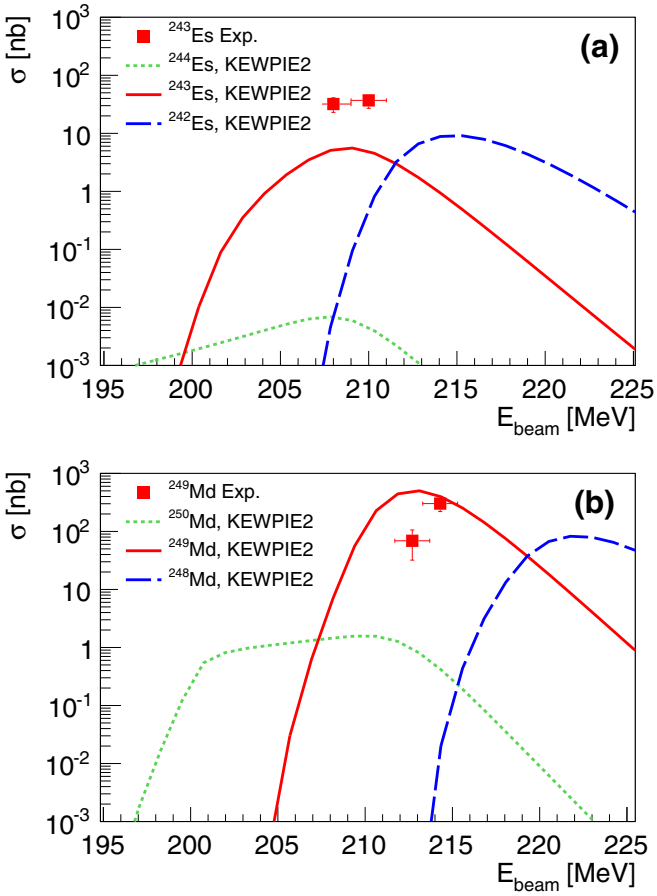

FIG. 8. Comparison between the experimental production cross sections for (a) ^{243}Es obtained in the present paper and the calculations of the $1n$, $2n$, and $3n$ cross sections performed with the KEWPIE2 code using the default parameters (macroscopic part described by the Thomas-Fermi parametrization as proposed by Myers-Świątecki [39] and the microscopic part based on the FRDM shell corrections [40]). (b) The same for ^{249}Md.

calculation reproduces the measured production cross sections well, whereas it underestimates them by a factor of 5 for the ^{243}Es case. The discrepancy for this latter case cannot be explained by a failure of the fusion model. Indeed, for a beam energy corresponding to the present measurement ($E_{\mathrm{cm}} \approx$ 169 MeV), the fusion model provides a fusion cross section $\sigma_{\mathrm{fus}} = 55$ mb in good agreement with the measurement $\sigma_{\mathrm{fus}} =$ 42 mb of Ref. [44]. Moreover, a discussion of the fusion cross section for the ^{48}Ca + ^{208}Pb reaction for which the WKB approximation provides a good description without fusion hindrance considerations can be found in Ref. [4]. In Fig. 9, the fission-barrier heights or the reduced friction parameters have been increased in order to reproduce the measurements for the $2n$ evaporation channel. Concerning the fission-barrier heights, it is necessary to add 500 keV to the absolute value of the shell corrections [with the liquid-drop fission barrier kept unchanged, see Eq. (3)] to obtain good agreement between the calculations and the data. Furthermore, the reduced friction parameter has to be increased by a factor of 3, i.e., to $\beta = 6 \times 10^{21}$ s^{-1} in order to obtain the same agreement.

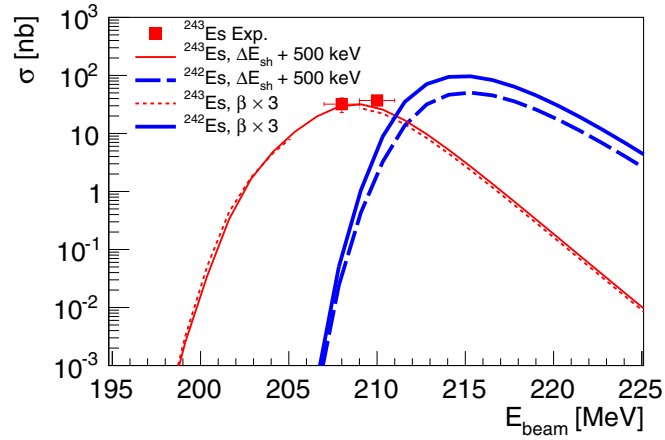

FIG. 9. Comparison between the experimental production cross sections for ^{243}Es extracted in the present paper and the calculations performed with the KEWPIE2 code considering either an adjustment of +500 keV of the barrier heights or an adjustment of the reduced friction parameter to $\beta = 6 \times 10^{21}$ s^{-1}.

It should be stressed that these adjustments remain within the uncertainty intervals for these parameters as discussed in Refs. [4,43]. Moreover, no theoretical model can presently predict the fission-barrier heights with an accuracy better than 0.5–1 MeV [45–47]. In the SHN region, differences between the models can be as large as 4 MeV [48]. Consequently, we cannot attribute the discrepancy observed for ^{243}Es (Fig. 8) to any specific parameters used in the KEWPIE2 code nor to any inputs from other nuclear models, in particular, those related to the fission process. Hence, the measured production cross sections for the ^{243}Es and ^{249}Md isotopes can be fully explained within the uncertainties in nuclear models and phenomenological parametrizations implemented in the KEWPIE2 code.

A way to provide constraints on the parameters used in the KEWPIE2 code would be to use more precise measurements in the VHN and SHN mass regions for a whole set of different evaporation channels, including a large scan in excitation energy for each of them. Indeed, using relevant data can help to fix and/or eliminate the impact of a specific parameter. Such an approach based on the Bayesian inference is discussed in Refs. [4,49].

VI. CONCLUSION

The odd-Z ^{243}Es and ^{249}Md were produced in the ^{197}Au(^{48}Ca, $2n$)^{243}Es and ^{203}Tl(^{48}Ca, $2n$)^{249}Md fusion-evaporation reactions, respectively. The half-life of ^{243}Es, ^{249}Md and its daughter ^{245}Es were measured, and the results were found compatible with those obtained in previous measurements following the α decay of heavier nuclei. The precisions of the half-lives of ^{249}Md and ^{245}Es were increased as well as those of the α-decay-branching ratios for those nuclei.

Production cross sections of ^{243}Es and ^{249}Md have been measured for the first time using ^{48}Ca-induced reactions and compared to the calculations performed with the KEWPIE2 code [4].

ACKNOWLEDGMENTS

We acknowledge the accelerator staff at the University of Jyväskylä for delivering a high-quality beam during the experiments. The Au targets were kindly provided by GSI. Support has been provided by the EU 7th Framework Programme "Integrating Activities-Transnational Access" Project No. 262010 (ENSAR) and by the Academy of Finland under the Finnish Centre of Excellence Programme (Nuclear and Accelerator Based Physics Programme at JYFL Contract No. 213503).

[1] D. Ackermann and C. Theisen, Phys. Scr. **92**, 083002 (2017).
[2] M. Asai, F. Heßberger, and A. Lopez-Martens, Nucl. Phys. A **944**, 308 (2015).
[3] C. Theisen, P. T. Greenlees, T.-L. Khoo, P. Chowdhury, and T. Ishii, Nucl. Phys. A **944**, 333 (2015).
[4] H. Lü, A. Marchix, Y. Abe, and D. Boilley, Comput. Phys. Commun. **200**, 381 (2016).
[5] M. Leino, J. Äystö, T. Enqvist, P. Heikkinen, A. Jokinen, M. Nurmia, A. Ostrowski, W. Trzaska, J. Uusitalo, K. Eskola, P. Armbruster, and V. Ninov, Nucl. Instrum. Methods Phys. Res., Sect. B **99**, 653 (1995).
[6] J. Sarén, J. Uusitalo, M. Leino, and J. Sorri, Nucl. Instrum. Methods Phys. Res., Sect. A **654**, 508 (2011).
[7] R. D. Page, A. N. Andreyev, D. E. Appelbe, P. A. Butler, S. J. Freeman, P. T. Greenlees, R.-D. Herzberg, D. G. Jenkins, G. D. Jones, P. Jones *et al.*, Nucl. Instrum. Methods Phys. Res., Sect. B **204**, 634 (2003).
[8] I. H. Lazarus, D. E. Appelbe, P. A. Butler, P. J. Coleman-Smith, J. R. Cresswell, S. J. Freeman, R. D. Herzberg, I. Hibbert, D. T. Joss, S. C. Letts *et al.*, IEEE Trans. Nucl. Sci. **48**, 567 (2001).
[9] P. Rahkila, Nucl. Instrum. Methods Phys. Res., Sect. A **595**, 637 (2008).
[10] J. Pakarinen, P. Papadakis, J. Sorri, R. D. Herzberg, P. T. Greenlees, P. A. Butler, P. J. Coleman-Smith, D. M. Cox, J. R. Cresswell, P. Jones *et al.*, Eur. Phys. J. A **50**, 53 (2014).
[11] P. Eskola, K. Eskola, M. Nurmia, and A. Ghiorso, Phys. Fenn. **8**, 357 (1973).
[12] Y. Hatsukawa, T. Ohtsuki, K. Sueki, H. Nakahara, I. Kohno, M. Magara, N. Shinohara, H. L. Hall, R. A. Henderson, C. M. Gannet *et al.*, Nucl. Phys. A **500**, 90 (1989).
[13] S. Antalic, F. P. Heßberger, S. Hofmann, D. Ackermann, S. Heinz, B. Kindler, I. Kojouharov, P. Kuusiniemi, M. Leino, B. Lommel, R. Mann, and Š. Šáro, Eur. Phys. J. A **43**, 35 (2010).
[14] H. W. Gäggeler, D. T. Jost, A. Türler, P. Armbruster, W. Brüchle, H. Folger, F. P. Heßberger, S. Hofmann, G. Münzenberg, V. Ninov *et al.*, Nucl. Phys. A **502**, 561 (1989).
[15] M. E. Leino, S. Yashita, and A. Ghiorso, Phys. Rev. C **24**, 2370 (1981).
[16] K. H. Schmidt, Eur. Phys. J. A **8**, 141 (2000).
[17] P. Eskola, Phys. Rev. C **7**, 280 (1973).
[18] F. P. Heßberger, G. Münzenberg, S. Hofmann, Y. K. Agarwal, K. Poppensieker, W. Reisdorf, K. H. Schmidt, J. R. H. Schneider, W. F. W. Schneider, H. J. Schött *et al.*, Z. Phys. A **322**, 557 (1985).
[19] J. M. Gates, S. L. Nelson, K. E. Gregorich, I. Dragojević, C. E. Düllmann, P. A. Ellison, C. M. Folden III, M. A. Garcia, L. Stavsetra, R. Sudowe, D. C. Hoffman, and H. Nitsche, Phys. Rev. C **78**, 034604 (2008).
[20] F. P. Heßberger, S. Hofmann, D. Ackermann, V. Ninov, M. Leino, G. Münzenberg, S. Saro, A. Lavrentev, A. G. Popeko, A. V. Yeremin *et al.*, Eur. Phys. J. A **12**, 57 (2001).
[21] F. Heßberger, S. Hofmann, B. Streicher, B. Sulignano, S. Antalic, D. Ackermann, S. Heinz, B. Kindler, I. Kojouharov, P. Kuusiniemi *et al.*, Eur. Phys. J. A **41**, 145 (2009).
[22] B. Streicher, Synthesis and spectroscopic properties of Synthesis and spectroscopic properties of transfermium isotopes with Z = 105, 106 and 107, Ph.D. thesis, Cornelius University, Bratislava, 2006.
[23] W. Brüchle, Radiochim. Acta **91**, 71 (2003).
[24] K. Abusaleem, Nucl. Data Sheets **112**, 2129 (2011).
[25] F. P. Heßberger, S. Antalic, D. Ackermann, Z. Kalaninová, S. Heinz, S. Hofmann, B. Streicher, B. Kindler, I. Kojouharov, P. Kuusiniemi *et al.*, Eur. Phys. J. A **48**, 75 (2012).
[26] G. Audi, F. G. Kondev, M. Wang, W. Huang, and S. Naimi, Chin. Phys. C **41**, 030001 (2017).
[27] F. P. Heßberger, S. Hofmann, D. Ackermann, P. Cagarda, R.-D. Herzberg, I. Kojouharov, P. Kuusiniemi, M. Leino, and R. Mann, Eur. Phys. J. A **22**, 417 (2004).
[28] J. Khuyagbaatar, F. P. Heßberger, S. Hofmann, D. Ackermann, V. S. Comas, S. Heinz, J. A. Heredia, B. Kindler, I. Kojouharov, B. Lommel *et al.*, Eur. Phys. J. A **46**, 59 (2010).
[29] J. Konki, B. Sulignano, P. T. Greenlees, C. Theisen, K. Auranen, H. Badran, R. Briselet, D. M. Cox, F. Defranchi Bisso, J. Dobaczewski *et al.*, Phys. Rev. C **97**, 024306 (2018).
[30] H. Gäggeler, T. Sikkeland, G. Wirth, W. Brüchle, W. Bögl, G. Franz, G. Herrmann, J. V. Kratz, M. Schädel, K. Sümmerer, and W. Weber, Z. Phys. A **316**, 291 (1984).
[31] J. E. Bastin, R.-D. Herzberg, P. A. Butler, G. D. Jones, R. D. Page, D. G. Jenkins, N. Amzal, P. M. T. Brew, N. J. Hammond, R. D. Humphreys *et al.*, Phys. Rev. C **73**, 024308 (2006).
[32] A. Chatillon, C. Theisen, E. Bouchez, P. A. Butler, E. Clément, O. Dorvaux, S. Eeckhaudt, B. J. P. Gall, A. Görgen, T. Grahn *et al.*, Phys. Rev. Lett. **98**, 132503 (2007).
[33] D. Peterson, B. B. Back, R. V. F. Janssens, T. L. Khoo, C. J. Lister, D. Seweryniak, I. Ahmad, M. P. Carpenter, C. N. Davids, A. A. Hecht *et al.*, Phys. Rev. C **74**, 014316 (2006).
[34] Y. T. Oganessian, V. K. Utyonkov, Y. V. Lobanov, F. S. Abdullin, A. N. Polyakov, I. V. Shirokovsky, Y. S. Tsyganov, A. N. Mezentsev, S. Iliev, V. G. Subbotin *et al.*, Phys. Rev. C **64**, 054606 (2001).
[35] I. Dragojević, K. E. Gregorich, C. E. Düllmann, M. A. Garcia, J. M. Gates, S. L. Nelson, L. Stavsetra, R. Sudowe, and H. Nitsche, Phys. Rev. C **78**, 024605 (2008).
[36] G. Münzenberg, S. Hofmann, H. Folger, F. P. Heßberger, J. Keller, K. Poppensieker, B. Quint, W. Reisdorf, K. H. Schmidt, H. J. Schött *et al.*, Z. Phys. A **322**, 227 (1985).
[37] G. Münzenberg, P. Armbruster, S. Hofmann, F. P. Heßberger, H. Folger, J. G. Keller, V. Ninov, K. Poppensieker, A. B. Quint, W. Reisdorf *et al.*, Z. Phys. A **333**, 163 (1989).
[38] N. Sato, H. Haba, T. Ichikawa, D. Kaji, Y. Kudou, K. Morimoto, K. Morita, K. Ozeki, T. Sumita, A. Yoneda *et al.*, J. Phys. Soc. Jpn. **80**, 094201 (2011).
[39] W. D. Myers and W. J. Świątecki, Phys. Rev. C **60**, 014606 (1999).

[40] P. Möller, J. R. Nix, W. D. Myers, and W. J. Swiatecki, At. Data Nucl. Data Tables **59**, 185 (1995).
[41] V. Weisskopf, Phys. Rev. **52**, 295 (1937).
[42] N. Bohr and J. A. Wheeler, Phys. Rev. **56**, 426 (1939).
[43] H. Lü, D. Boilley, Y. Abe, and C. Shen, Phys. Rev. C **94**, 034616 (2016).
[44] A. J. Pacheco, J. O. Fernández Niello, D. E. DiGregorio, M. di Tada, J. E. Testoni, Y. Chan, E. Chávez, S. Gazes, E. Plagnol, and R. G. Stokstad, Phys. Rev. C **45**, 2861 (1992).
[45] F. P. Heßberger, Eur. Phys. J. A **53**, 75 (2017).
[46] R. Capote, M. Herman, P. Obložinský, P. G. Young, S. Goriely, T. Belgya, A. V. Ignatyuk, A. J. Koning, S. Hilaire, V. A. Plujko *et al.*, Nucl. Data Sheets **110**, 3107 (2009).
[47] M. Kowal, P. Jachimowicz, and A. Sobiczewski, Phys. Rev. C **82**, 014303 (2010).
[48] A. Baran, M. Kowal, P.-G. Reinhard, L. M. Robledo, A. Staszczak, and M. Warda, Nucl. Phys. A **944**, 442 (2015).
[49] H. Lü and D. Boilley, EPJ Web Conf. **62**, 03002 (2013).